Kinematics and wing shape across flight speed in the bat, *Leptonycteris yerbabuenae*

Rhea von Busse[1,*,‡], Anders Hedenström[2], York Winter[1] and L. Christoffer Johansson[2]

[1]Cognitive Neurobiology, Department of Biology, Humboldt University, Dorotheenstr.94, 10117 Berlin, Germany
[2]Department of Biology, Lund University, Sölvegatan 37, SE-22362 Lund, Sweden

*Present address: Department of Ecology and Evolutionary Biology, Brown University, 34 Olive St, Providence, RI 02912, USA
‡Author for correspondence (rhea@vonbusse.de)

Biology Open 1, 1226–1238
doi: 10.1242/bio.20122964
Received 29th August 2012
Accepted 10th September 2012

Summary

The morphology and kinematics of a flying animal determines the resulting aerodynamic lift through the regulation of the speed of the air moving across the wing, the wing area and the lift coefficient. We studied the detailed three-dimensional wingbeat kinematics of the bat, *Leptonycteris yerbabuenae*, flying in a wind tunnel over a range of flight speeds (0–7 m/s), to determine how factors affecting the lift production vary across flight speed and within wingbeats. We found that the wing area, the angle of attack and the camber, which are determinants of the lift production, decreased with increasing speed. The camber is controlled by multiple mechanisms along the span, including the deflection of the leg relative to the body, the bending of the fifth digit, the deflection of the leading edge flap and the upward bending of the wing tip. All these measures vary throughout the wing beat suggesting active or aeroelastic control. The downstroke Strouhal number, St_d, is kept relatively constant, suggesting that favorable flow characteristics are maintained during the downstroke, across the range of speeds studied. The St_d is kept constant through changes in the stroke plane, from a strongly inclined stroke plane at low speeds to a more vertical stroke plane at high speeds. The mean angular velocity of the wing correlates with the aerodynamic performance and shows a minimum at the speed of maximum lift to drag ratio, suggesting a simple way to determine the optimal speed from kinematics alone. Taken together our results show the high degree of adjustments that the bats employ to fine tune the aerodynamics of the wings and the correlation between kinematics and aerodynamic performance.

Key words: *Leptonycteris yerbabuenae*, Bat, Kinematics, Flight, Wing shape, Wind tunnel, Leading edge flap

Introduction

Bat wings show the most varied in-flight wing morphology of the three extant animal taxa, i.e. bats, birds and insects, which have evolved active flight. Their wings are made from a highly compliant wing membrane and flexible wing bones (Swartz, 1997). The forelimb bones are elongated relative to non-volant animals (Swartz et al., 1996). Additionally, the bone mineralization is reduced and the cortical thickness is increased distally (Swartz and Middleton, 2008). This combination of geometry and mineralization increases the deformability of the wing bones during flight and reduces the mass moment of inertia and potentially the inertial power of flight (Thollesson and Norberg, 1991; Swartz, 1997). The wing membrane shows a strong anisotropy, with maximum stiffness and strength parallel to the wing chord and greatest extensibility parallel to the trailing edge of the wing (Swartz et al., 1996). In addition, the different regions of the membrane show a high variation in load capacity and extensibility (Swartz et al., 1996; Swartz and Middleton, 2008). The wing also contains intrinsic muscles, unique to bats, which may control the mechanical properties of the membrane (e.g. Norberg, 1972). Consequently, the bat wing morphology suggests a high potential for ability to adjust wing morphology according to the aerodynamic demands, but present difficulties in studying bat flight kinematics not encountered in birds or insects.

Due to the strong dependency of the generated aerodynamic lift on flight speed of a wing, bats are expected to alter their kinematics and wing morphology across flight speeds to generate sufficient weight support and thrust. When flight speed is reduced sustaining weight support becomes more demanding and the bats need to compensate for the lower velocity over the wings by increasing the wing area, flapping speed or lift coefficient. This is particularly important during very slow and hovering flight. A general mechanism for increasing the lift coefficient is to increase the angle of attack (*AoA*). In addition, potential high-lift features, such as high camber of the wing (Norberg, 1972; Laitone, 1997) and the use of leading edge vortices (Muijres et al., 2008) are well known mechanisms to increase the lift coefficient. We measured standard kinematic parameters such as wing beat frequency, amplitude and angle of attack as well as parameters related to the varying morphology of the wing. To capture the high flexibility and deformation of the bat wing, we measured the angles between the wing bones, which are related to the wing area, the bend and sweep of the wing tip, which are indicators of the aeroelastic morphing of the wing, and different measures of the camber of the wing along the span, which is related to the lift coefficient of the wing.

The bat species used in this study, *L. yerbabuenae*, is a nectar-feeding species that hovers during flower visits. However, *L. yerbabuenae* also makes long commuting flights, around 100 km every night, between its roosting and feeding sites (Horner et al., 1998). In addition, *L. yerbabuenae* migrates annually up to 1000–1600 km between southern Mexico and southern Arizona, which is among the longest known migration routes in bats (Wilkinson and Fleming, 1996). This suggests selection for efficient flight. Comparison with the performance of another related, non-migratory, species (*Glossophaga soricina*) have suggested adaptations in optimal flight speed related to the difference in flight behavior (Muijres et al., 2011). Here we explore how kinematics and wing morphology is controlled across flight speed and if aerodynamic performance can be related to kinematics.

Materials and Methods

Animals

Two individuals of the tropical nectar-feeding bat *Leptonycteris yerbabuenae* were used in this study (same individuals as used in Muijres et al. (Muijres et al., 2011)). Morphological measurements were made on in-flight images during the middle of the downstroke (Image J, http://rsb.info.nih.gov/ij) following Pennycuick (Pennycuick, 1989a). We measured the semi-span b, defined as half the full (tip-to-tip) wing span and the wing area S, including the body area between the wings. Using these parameters the mean chord $c=S/2b$, the non-dimensional aspect ratio $AR=4b^2/S$ and the wing loading $Q=mg/S$ was calculated, where m is the body mass and g the gravitational acceleration (Table 1). The nocturnal bats were clock-shifted 12 h so that their active period (night) coincided with that of experimenters. Between experiments the bats were kept in a facility where they could fly freely and had access to honey water, with and without supplementary food (Nectar-Plus [Nekton, Pforzheim, Germany], baby formula), and pollen *ad libitum*. The temperature in the housing facility was kept at 25±2℃ (mean ± SD) and the humidity was kept around 60%.

Experimental set-up

The experiments were performed in the low-turbulence wind tunnel at Lund University (Pennycuick et al., 1997). During the experiments the mean temperature in the wind tunnel was 22.6℃, mean air density 1.18 kg/m^3 and mean air pressure 1002 hPa.

The bats were trained to feed from a small metal tube (2 mm diameter) suspended from the ceiling of the wind tunnel (supplementary material Fig. S1). During resting periods the bats were roosting on a net 6 m upstream of the test section in the settling chamber. During feeding flights the bats would fly into the test section with the wind and perform a U-turn to approach the feeder from downstream. During the feeder visits the bats were flying steadily in front of the feeder opening, which allowed for controlled and repeatable flight measurements at fixed speeds.

Kinematic sequences were recorded for the following flight speeds: 0 m/s, 1.0 m/s, 1.5 m/s, 2.0 m/s, 2.5 m/s, 3.0 m/s, 3.5 m/s, 4.0 m/s, 5.0 m/s, 6.0 m/s and 7.0 m/s. The bats were filmed with two synchronized high-speed cameras (Redlake, MotionScope PCI 500, frame rate 250 Hz, shutter speed 1/1250 s) from ventral [x–y] and side [x–z] views. The coordinate system was right handed, defined as: x, in the direction of the flow; y, transverse to the flow; z, vertical (supplementary material Fig. S1). To minimize distraction of the bats the test section was illuminated by infrared lights (VDI-IR607, Video Security Inc., Taiwan).

Digitized markers

17 natural body and wing markers (Fig. 1) were digitized in both views and transformed into three-dimensional coordinates by direct linear transformation (DLT), using Matlab® routines (courtesy of Christoph Reinschmidt) (error estimate of the digitized body and wing coordinates in 3D can be found in supplementary material Table S1). The body and wing points (Fig. 1) are defined as follows and further referred to as neck [1], the lateral point of the neck; shoulder [2], the connection of the wing membrane to the body; elbow [3], the rearward tip of the elbow; wrist [4], the point between thumb and leading edge of the wing; P(II)t [5], the tip of the second digit; P(III)i [6],the joint between the metacarpal and the first phalanx of the third digit; P(III)s [7], the joint between the first and second phalanges of the third digit; P(III)t [8], the joint between the second and third phalanges of the third digit; WT [9], the wing tip; P(IV)i [12], the joint between the metacarpal and the first phalanx of the fourth digit; P(IV)s [11], the joint between the first and second phalanges of the fourth digit; P(IV)t [10], the tip of the fourth digit; P(V)i [15], the joint between metacarpal and the first phalanx of the fifth digit; P(V)s [14], the joint between the first and second phalanges of the fifth digit; P(V)t [13], the tip of the fifth digit; foot [16], the connection of the wing membrane to the foot; and hip [17], the lateral end of the legs connecting to the hip.

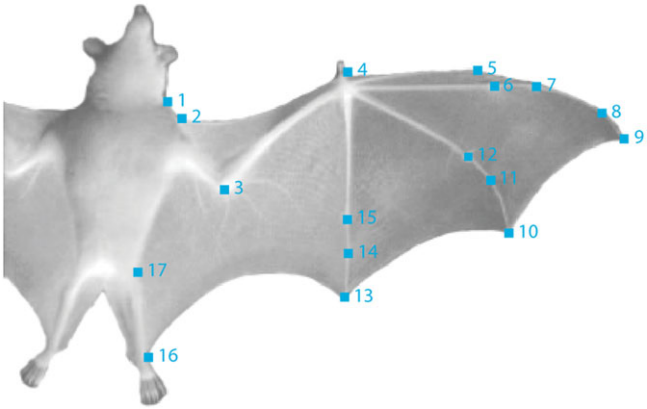

Fig. 1. Numbers corresponding to the digitized body and wing points in the study, as seen from below.

Kinematic parameters

Using the coordinate data of the markers, we estimated aerodynamically relevant parameters. The wingbeat frequency, f, was calculated using the power spectra of a Fourier transform of the vertical wingtip trace as a function of time. The inverse of the frequency, the wingbeat period, $T=1/f$, is divided into the period of the downstroke T_d and the period of the upstroke T_u estimated from the timing of the upper- and lower-most position of the wing tip. The downstroke ratio, τ, is defined as the downstroke fraction of one wingbeat cycle $\tau=T_d/T$. We estimated the wingbeat amplitudes along the three dimensions, A_x (in direction of the flow), A_y (in horizontal direction, perpendicular to the flow) and A_z (in vertical direction), as the excursion of the wingtip relative to the shoulder. The stroke plane angle, β, is the angle between a line connecting the wingtip in the upper- and lower-most position in the side view [xz] relative to the horizontal (Fig. 2). The angular amplitude, θ, is defined as the angle between the upper- and lower-most position of the wingtip measured within the stroke plane. The angles of attack are calculated for different sections of the wing as the angles between the following triangular planes and the velocity vector, relative to still air, of the centroid of each triangle. The outer wing, the *dactylopatagium*, triangle 3 (wrist–P(III)t–P(V)t [pts 4–9–13]), the inner most part of the wing controlled by the elbow movement, triangle 5 (shoulder–elbow–foot [pts 2–3–16]), and the two inner wing triangles 7 (shoulder–P(V)t–foot [pts 2–13–16]) and 8 (shoulder–wrist–P(V)t [pts 2–4–13]) (Fig. 1). The maximal and mean angles of attack are calculated during the downstroke for triangle 3 (Fig. 1). From the measures of frequency, amplitude and flight speed (U) we calculated the *Strouhal* number (St) as $St=fA_z/U$. The *Strouhal* number during the downstroke, St_d, was calculated following Wolf et al. (Wolf et al., 2010):

$$St_d = \frac{\frac{fA_z}{2\tau}}{U + \frac{fA_x}{\tau}}$$

Table 1. Morphometric data for the two individuals.

Measure	Symbol	Units	Bat M (male)	Bat F (female)
Mean body mass	m	g	21.6	23.0
Forearm length		cm	5.03	5.10
Span	$2b$	cm	33.5	32.3
Wing area	S	cm^2	157.6	152.9
Mean chord	c	cm	4.7	4.7
Aspect ratio	AR		7.1	6.8
Wing loading	Q	N/m^2	13.4	14.7

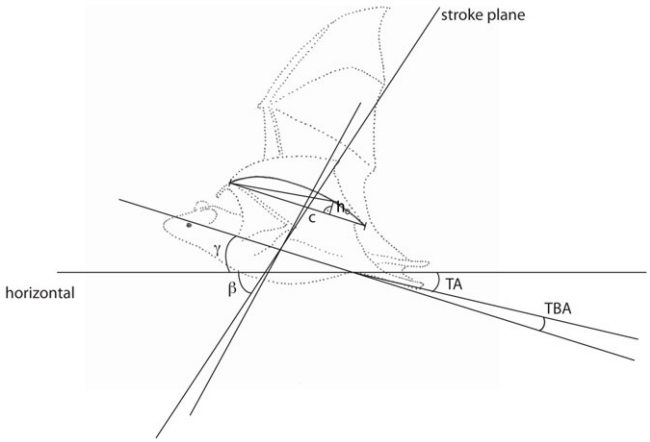

Fig. 2. Definition of kinematics parameters: the stroke plane angle β relative to the horizon, the body and tail tilt angles γ and *TA* relative to the horizon, the tail angle relative to the body, *TBA*, the wing chord c and the height of the cambering h_c. The latter two variables allowed us to calculate the camber: h_c/c.

In addition to the motion related parameters above, we also estimated parameters describing the morphology of the wings. The inner wing area, S_i, is the sum of the two triangular areas between the wrist, the P(V)t and the foot [pts 4–13–16] and the wrist, the shoulder and the foot [pts 4–2–16] (Fig. 1). As alternative measures of the spreading of the wings, we measured the angles between the fingers and arm bones, *H/R*, *R/PV*, *PV/IV* and *PIV/III*, which are the 3D angles between the humerus (the shoulder–elbow line [pt 2–3]) and the radius (the elbow–wrist line [pt 3–4]), between the radius and the 5th digit (the wrist–P(V)i line [pt 4–15]), between the 5th digit and the 4th digit (the wrist–P(IV)i line [pt 4–12]) and between the 4th digit and the 3rd digit (the wrist–P(III)i line [pt 4–6]) respectively (Fig. 1). The span ratio, *SR*, is defined as the span at mid-upstroke divided by the span at mid-downstroke. We determined the sweep of the wing tip as the in-plane flexion of the wingtip and estimated it as the angle between the wrist–WT line [pt 4–9] and the wrist–P(III)i line in the plane of the triangle wrist–P(III)i–P(IV)i [pts 4–6–12] (Fig. 3). Backwards directed sweep is indicated by negative sweep angles. To get a measure of the aeroelastic deformation of the wing we measured the bend of the wing tip as the out of plane deflection of the wingtip relative to the hand wing. Bend is defined as the angle between the wrist–WT line [pt 4–9] and the plane of the triangle wrist–P(III)i–P(IV)i [pts 4–6–12] (Fig. 3). Negative bend angles indicate a downward directed bend. We also measured parameters relating to the camber or curvature of the wing profile. The inner-most part of the wing is controlled by the position of the feet relative to the body. We estimated the body tilt angle, γ, as the angle between the shoulder–hip line and the horizontal (Fig. 2) (a positive body tilt angle indicates a nose-up directed body) and the tail angle, *TA*, as the angle between the hip–foot line and the horizontal (Fig. 2) (downwards directed feet are indicated by a positive tail tilt angle). From these two estimates we calculated the relative tail to body angle, *TBA*, as γ-*TA* (Fig. 2) as a measure of the camber of the inner wing. The camber of the mid wing is calculated as the perpendicular distance from the chord (wrist–P(V)t [pt4–13] to the point P(V)i [pt 15] divided by the length of the chord. The camber is generated by flexion of the phalanges of the 5th digit and is described by the angles PVs (between the wrist–P(V)i line [pt 4–15] and the P(V)i–P(V)s line [pt 15–14] relative to the inner wing plane) and PVt (the angle between the P(V)i–P(V)s line [pt 15–14] and the P(V)s–P(V)t line [pt 14–13] relative to the inner wing plane) (Fig. 2). In addition, the *dactylopatagium brevis* (the membrane between the thumb, the wrist and P(II)t) and *dactylopatagium minor* (the membrane between the wrist, P(II)t and P(III)s) have been suggested to function as a leading edge flap partly controlling the camber of the outer wing. We estimated the leading edge angle, *LE*, as the angle of the leading edge flap (wrist–P(II)t–P(III)i [pts 4–5–6]) relative to the triangle wrist–P(III)i–P(IV)i [pts 4–6–12] (Figs 1, 3). A downward deflected leading-edge flap is indicated by positive leading edge angles.

Statistics

We analyzed two to eight wingbeats of three to four stable sequences for each bat and speed. In total 176 wingbeats were analyzed. The analyzed sequences were divided into single wingbeats from the beginning of the downstroke to the end of the upstroke. The beginning and end of a half-stroke were defined by the upper-most and lower-most turning point of the wingtip relative to the shoulder. Each downstroke and upstroke was normalized over time and we used a spline function to generate the average number of data-points for each downstroke and upstroke (at each speed). The individual wingbeats were then used to generate mean curves, with error estimates over time using a nested ANOVA (Matlab® function, anovan) with sequence as random factor.

For all statistical tests we used mixed linear models using the GLM procedure in JMP 8.0 (SAS Institute, Cary, North Carolina, USA) with reduced maximum likelihood estimates (REML) of the variance, which produce unbiased estimates of variance and covariance parameters (Kenward and Roger, 1997). The model was constructed including the dependent variable (Y), individual, sequence (nested within individual and set as random factor to address the repeated measures set-up of the experiment) with the flight speed (U) as a covariate. The model also included the interaction between individual and speed. The relationship between the variable of interest and the covariate were tested as linear, second or third order polynomial functions and the highest level of non-significant terms were successively removed. When individual differences were significant the fitted curves, based on the parameter estimates in the test, for each individual are shown, otherwise the combined data for both individuals are presented. For example, for individual one the fitted function was estimated as:

$$Y = Y_0 + (a + a_{i1})U + (b + b_{i1})U^2 + (c + c_{i1})U^3$$

where Y_0 is the intercept, a the linear coefficient, a_{i1} the interaction effect of individual 1 on the linear coefficient, b the quadratic coefficient, b_{i1} the interaction effect of individual 1 on the quadratic coefficient, c the cubic coefficient, c_{i1} the interaction effect of individual 1 on the cubic coefficient. Presented r^2 and p-values refer to the overall model fit of the mixed model and functions presented are from the mixed model fit. Using REML to estimate the variance result in the F-statistics and degrees of freedom not being estimated in the traditional way and they are therefore not presented. Graphs were plotted in OriginPro 8 (OriginLab Corporation, Northampton, USA). The data are presented in means ± S.E.M.

Results

Wing movement

The wing movements change continuously from slow to high speeds. The wing moves from a position above and behind the shoulder to a position below and in front of the shoulder during the downstroke, describing an elliptic curve when seen from the side (Fig. 4d–f). At slow speeds the wing shows a more horizontally-directed stroke plane while at higher speed a more vertical stroke plane (Fig. 4d–f). The change in stroke plane is associated with a decrease in body tilt angle with increasing speed, which can be seen in the position of the foot relative to the shoulder and by comparing the position of the wrist to the path of P(V)t (Fig. 4g–i). The wing span during the upstroke is less compared to the wingspan during the downstroke at low speeds compared to high speeds (Fig. 4a–c), indicating a lower span ratio at low speeds.

With increasing speed the vertical amplitude increases, which is apparent in the rear view (Fig. 4g–i), while the horizontal amplitude decreases (Fig. 4d–f). The movement of the tip of the

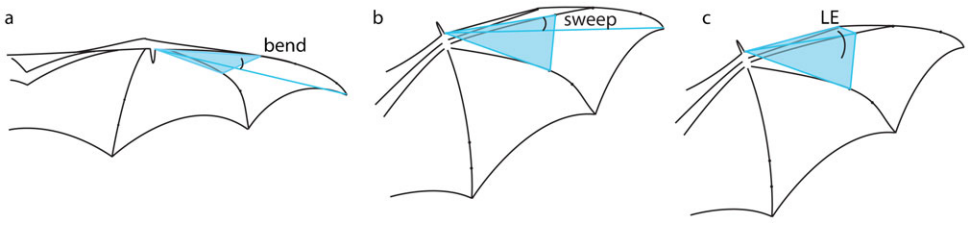

Fig. 3. Illustration of a bat wing seen from the front (**a**) and from below (**b**,**c**) to visualize the wing tip excursion in the out of plane direction, bend (a), in the in-plane direction, the sweep (b), and the angle of the leading edge flap (c). All measures are relative to the plane formed by the points 4, 6 and 12 (Fig. 1).

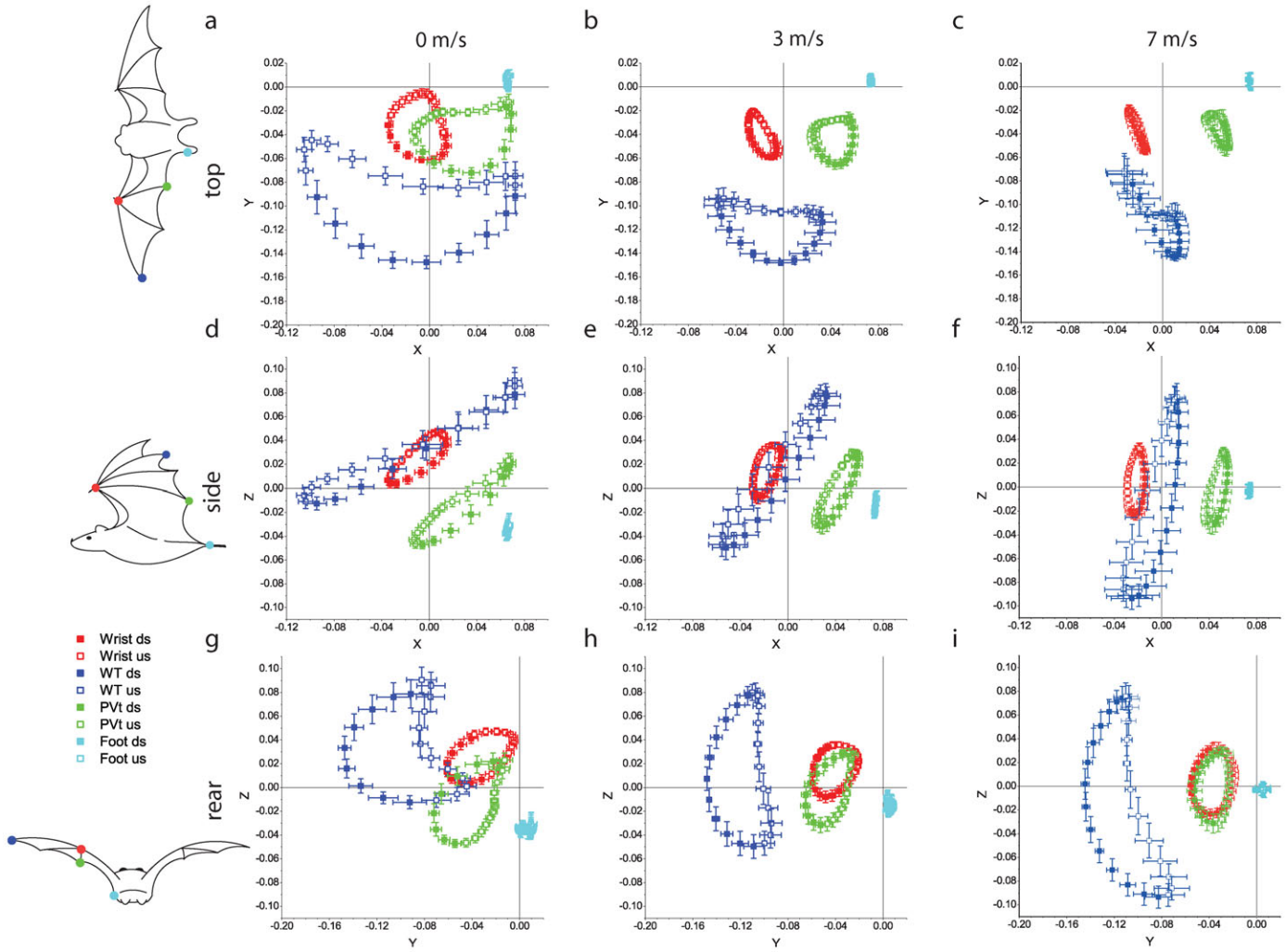

Fig. 4. The wing movement relative to the shoulder is shown for three different speeds (**a**,**d**,**g**: slow [0 m/s]; **b**,**e**,**h**: intermediate [3 m/s]; **c**,**f**,**i**: high [7 m/s]) and three different views (a,b,c: from above; d,e,f: the side; g,h,i: behind the flying animal). The trace of the wrist, the wingtip, the tip of the 5th finger and the foot are mapped with the shoulder as the origin. Filled symbols represent the downstroke, open symbols the upstroke. The points are species means ± S.E.M. for the mean number of frames during a wing beat at each speed (see Materials and Methods). All distances are shown in m.

5th digit also shows an elliptic path, as seen from the side, similar to the wrist, but the ellipse has a slightly larger diameter (Fig. 4d–f). The difference is more pronounced at low speed and indicates a higher amplitude of the trailing edge than the leading edge, which suggests a rotation around an axis parallel to the wing span.

Amplitudes

The angular amplitude in the stroke plane, θ, follows a U-shaped pattern with high values at low flight speed with decreasing and then increasing values with increasing speed. The angular amplitude varies with the square of the flight speed ($r^2=0.42$, $P<0.0001$), with significant difference between the two bats ($P<0.0001$, $\theta=88.66-10.45U+1.34U^2$ for the male bat (batM) and $\theta=96.95-8.75U+1.14U^2$ for the female bat (batF)). θ is highest at low speeds at around 90° and 95°, drops to 65° and 75° at 3 m/s for batM and batF respectively and rises back to about 80° at high speeds for both bats (Fig. 5a).

The vertical amplitude, A_z, of the wingtip increases with increasing flight speed following a second order polynomial ($r^2=0.70$, $P<0.0001$). The two individuals differed significantly ($P<0.0001$, $A_z=0.0855+0.0134U-0.0004U^2$ for batM and $A_z=0.0982+0.0165U-0.0008U^2$ for batF) from 0.08 m and 0.10 m for batM and batF respectively at low speeds to around 0.17 m for both bats at high speeds (Fig. 5b).

Stroke plane angle

The stroke plane angle, β, increases from less than 30° at low to about 75° at high flight speed, indicating a change from a more horizontal to a more vertical stroke plane (Fig. 5c, Fig. 4d–f). The increase follows a third order polynomial ($r^2=0.95$, $P<0.0001$, $\beta=27.31+6.29U-1.58U^2-0.21U^3$) ± individual differences ($P>0.05$).

Span ratio

The span ratio, *SR*, increases when going from low to medium flight speed and then decreases slightly when flight speed is increased further. The *SR* varies with the square of the speed ($r^2=0.82$, $P<0.0001$), and the two individuals show significant

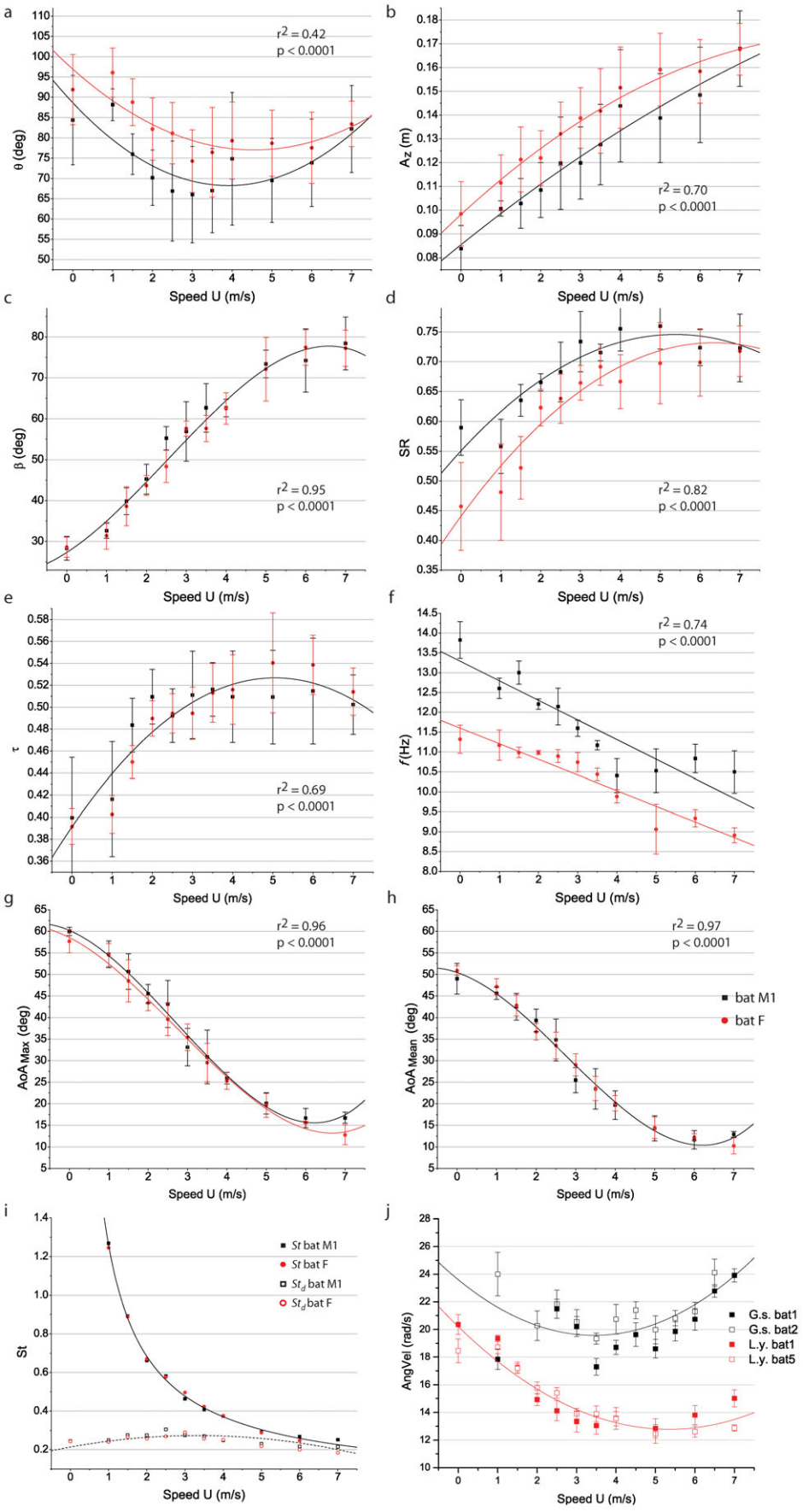

Fig. 5. Variation in kinematic parameters across flight speed, U [m/s]. The angular amplitude θ [°] (**a**), the vertical amplitude A_z [m] (**b**), the stroke plane angle β [°] (**c**), the span ratio SR (**d**), downstroke ratio τ (**e**), the wingbeat frequency f [Hz] (**f**), the maximal (**g**) and mean (**h**) angle of attack [°], Strouhal number St, filled symbols, and Strouhal number for the downstroke St_d, open symbols (**i**), with bat M in black squares and bat F in red circles; and mean angular velocity in radians per second over speed of *Leptonycteris yerbabuenae* in red and *Glossophaga soricina* in black symbols (**j**). All graphs show mean values ± S.E.M. for both bats for each speed U. The curves represent the best fit of the mixed linear model (see Materials and Methods). If significant individual differences were found, the best fit was calculated for the bats separately; otherwise they were combined. In j the curves represented with best fit for respective species.

differences ($P<0.0001$, $SR=0.551+0.073U-0.007U^2$ for batM and $SR=0.441-0.092U-0.007U^2$ for batF) (Fig. 5d). The span ratio starts at 0.59 for batM and 0.45 for batF during hovering flight. The values reach a level around 0.73 and 0.68 for batM and batF respectively at intermediate speeds (around 3 m/s) and increase up to approximately 0.73 for batF at higher speeds.

Downstroke ratio

The downstroke ratio, τ, increases when going from low to medium flight speed and then decreases slightly when flight speed is increased further (Fig. 5e) and follows a second order polynomial ($r^2=0.69$, $P<0.0001$, $\tau=0.391+0.054U-0.005U^2$) for both bats ($P>0.05$). The downstroke ratio starts at 0.40, quickly increases to 0.50 and levels out slightly above, at around 3 m/s.

Wingbeat frequency

The wingbeat frequency, f, decreases with increasing flight speed (Fig. 5f). The wing beat frequency is significantly different between the two individuals ($P<0.0001$) ($r^2=0.74$, $P<0.0001$, $f=13.29-0.49U$ for batM and $f=11.60-0.39U$ for batF). The wingbeat frequency of batM is 13.8 Hz during hovering flight and decreases to 10.5 Hz for intermediate and high speeds ($U=4$–7 m/s). BatF shows an almost constant wingbeat frequency around 11.0 Hz at low speeds ($U=0$–2.5 m/s), which decreases to 9.0 Hz at 7 m/s.

Strouhal number

The Strouhal number, St, initially has high values around 1.25 at 1 m/s and decreases asymptotically to values around 0.25 at 7 m/s for both bats (Fig. 5i). The Strouhal number during the downstroke, St_d, shows generally low values between 0.2 and 0.3, following a second order polynomial ($r^2=0.77$, $P<0.0001$, $St_d=0.25+0.019U-0.0039U^2$). The highest value occurs at 2.4 m/s.

Inner wing area

S_i varies sinusoidally over the wing beat with the largest S_i found during mid-downstroke (Fig. 6a). During this phase the wing area reaches 0.0050 m^2 for low speeds and 0.0040 m^2 for high speeds. At intermediate to high speeds the lowest S_i can be found in the middle of the upstroke, dropping to 0.0020 m^2. At low speeds, however, a partial increase in the S_i is visible at mid upstroke, making the lowest values approximately 0.0028 m^2.

Finger and arm angles

The arm angle *H/R* varies sinusoidally over the entire stroke (Fig. 6b). The highest angle is reached during mid-downstroke, approximately 100° at low speeds and around 75° at high speeds. The lowest angles are reached just after the beginning of the upstroke, with values around 30° for low and high speeds and 40° for intermediate speeds.

R/PV reaches maximal values, around 60° for low speeds and around 45° for high speeds, at the end of the downstroke (Fig. 6c). Minimal values are reached at mid upstroke, with lower values, around 20°, for low and high speeds and higher values, around 30°, for intermediate speeds.

At slow speeds the *PV/IV* angles during the downstroke are higher than at higher speeds and fluctuate slightly (around 59° for low speeds and around 56° for intermediate and high speeds) (Fig. 6d). Around mid-upstroke the angles decrease to 49° at low and intermediate speeds and 52° at high speeds.

The *PVI/III* angles stay around 30° for intermediate and high speeds throughout the stroke, but drop to 22° during mid-upstroke at low speeds (Fig. 6e).

Angle of attack

The angle of attack of the outer wing (*AoA3*, Fig. 7a) stays nearly constant during the downstroke, with higher values for lower speeds (~50° for low speeds and ~10° for high speeds) and decreases during the upstroke until mid-upstroke, with minimal values for low speeds (−70° for low speeds and −10° for high speeds). For all speeds the angle of attack is positive during the downstroke and negative during the upstroke.

The maximum and mean angle of attack decreases with increasing flight speed and follows a third order polynomial relative to flight speed. The maximum angle of attack reach values of 60° during the downstroke at low speeds and decrease continuously to ~15° over the speed range ($r^2=0.96$, $P<0.0001$) (Fig. 5g). The average angle of attack shows a similar pattern but starts around 50°, decreasing down to ~12° over the speed range ($t^2=0.97$, $P<0.0001$) (Fig. 5h). No individual differences could be found for the mean angle of attack ($P>0.05$, $AoA_{mean}=50.46-3.09U-2.13U^2+0.26U^3$), but the maximum angle of attack showed significant individual differences ($P=0.0033$, $AoA_{max}=60.21-3.92U-1.92U^2+0.27U^3$ for batM and $AoA_{max}=58.55-4.63U-1.68U^2+0.20U^3$ for batF).

The highest values of the angle of attack *AoA7* (Fig. 7b) are reached for hovering flight (80° to −60°). With increasing speed, the extension of the curves decreases. During the downstroke the angles are positive, while after mid-upstroke, the angles become negative for all speeds.

The *AoA8* shows a similar pattern than *AoA7*. At 0 and 1.0 m/s, *AoA8* reaches negative values during parts of the upstroke. For 1.0 m/s this occurs only at the beginning of the upstroke, but for 0 m/s *AoA8* is negative for almost the entire upstroke and reaches a minimum of −40°. At intermediate speeds the angles are positive throughout the entire stroke, with higher values during the downstroke: around 20° (Fig. 7c). At high speeds *AoA8* shows constant values around 2° throughout the wing beat.

Leading edge flap angle

The angle of the leading edge flap (*LE*) relative to the wing varies between the wingbeats at all speeds, as evidenced by the large error bars (Fig. 8a). However, the pattern is consistent at all speeds, with a positive *LE*-angle with more constant values during the downstroke (around 5° at high speeds and around 25° at low speeds) and a decrease during the upstroke with a negative minimum (~−10°) around mid-upstroke. At high speeds the entire upstroke shows negative values.

Camber of the fifth digit

The highest camber can be found at 1.5 m/s (Fig. 8b). At 1.0 and 0 m/s the camber is not as high as it is at 1.5 m/s, but it changes more during the downstroke with a peak at the end of the downstroke, around 0.16, decreasing to 0.10 and increasing again to an even higher value, around 0.22 at the end of the upstroke. At intermediate speeds the camber reaches values between 0.11 and 0.14. At high speeds the camber of the wing stays constant over time at around 0.04.

The angle *PVs* (Fig. 8c) shows a similar pattern to the camber of the fifth digit. At low speeds *PVs* changes the most, with a minimum around 20° at the beginning of the upstroke and a

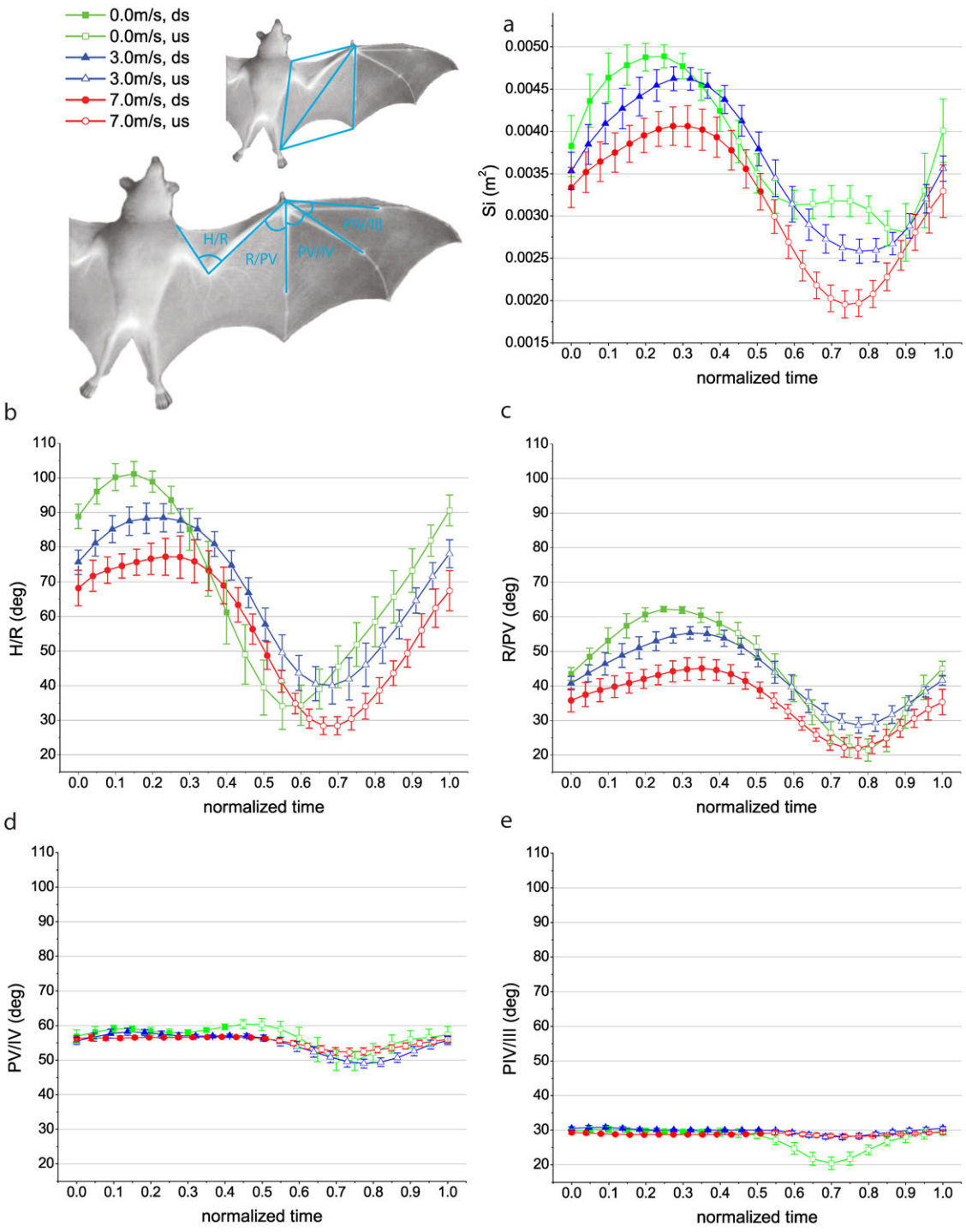

Fig. 6. Inner wing area and four wing angles are shown for three different speeds. The bat schemes illustrate the definition of the parameters. The inner wing S_i area (**a**) is presented in m^2, the finger angles *H/R* (**b**), *R/PV* (**c**), *PV/IV* (**d**) and *PIV/V* (**e**) in degrees. The time axes are normalized. The curves are species means ± S.E.M. (see Materials and Methods). Filled symbols represent the downstroke, open symbols the upstroke.

maximum, around 45° at the end of the upstroke. The highest values can be found at 1.5 m/s. At intermediate speeds *PVs* reaches values around 22° to 30°. At high speeds (5–7 m/s) the angle stays fairly constant, between 7° and 10°.

The angle *PVt* (data not shown) changes without clear pattern during the stroke. The values fluctuate between 0° and 10° for slow and intermediate speeds and lower values for high speeds (0° to 5°).

Bend and sweep

The bend follows a sinusoidal curve with a maximum around mid-downstroke and a minimum around mid-upstroke (Fig. 8d). The values for the downstroke vary for all speeds between −1° and −9°, with the lowest values for intermediate speeds. During the upstroke the bend drops to values between −14° and −16°; only at high speeds do the values stay higher, at around −10°.

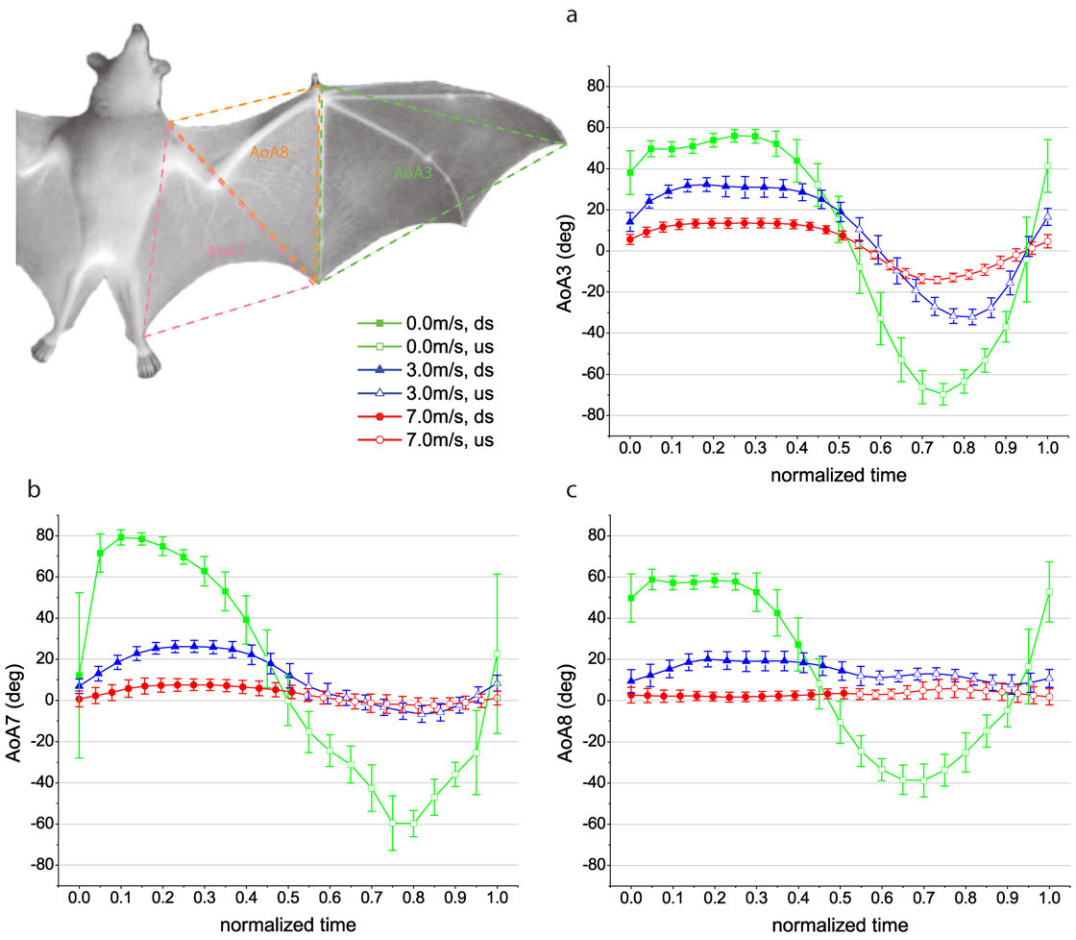

Fig. 7. Angles of attack are presented at three different speeds. The bat scheme illustrates the definition of the triangles. Three different angles of attack are shown: the outer wing triangle *AoA3* (**a**) and two inner wing triangles *AoA7* (**b**) and *AoA8* (**c**). The angles of attack are presented in degrees. The time axes are normalized. The curves are species means ± S.E.M. (see Materials and Methods). Filled symbols represent the downstroke; open symbols represent the upstroke.

At high speeds the sweep angle stays constant around −7° (Fig. 8e) throughout the wing beat. With decreasing speed the sweep becomes more negative and drops down to −9° at the beginning of the downstroke, rises (back to −7° for low speeds) and then drops again to a minimum at mid-upstroke at −12° for hovering speed.

Body and tail angles

The body angle varies relatively constant throughout the stroke across speeds (Fig. 8f) with a higher body angle at low speeds (between 15° and 20° at hovering flight). At intermediate speeds the body angle lies between −2.5° and 5° and at high speeds the body angle shows only negative values, between −7° and 0°, with the lowest values for 5 m/s.

During the downstroke the tail to body angle, *TBA*, increases and during the upstroke it decreases again. The mean *TBA* increases from low to medium flight speed and then decreases again as flight speed increases further following a second order polynomial function (r^2=0.87, P=0.0003, TBA=4.64+3.78U−0.63U^2). There is considerable variation throughout the wingbeat. At low speeds the values change from 0° to 12° and back to 0°; the maximal values are reached for 2.0 m/s, varying between 0° and 20°. At high speeds the *TBA* shows a different pattern, dropping down from 5° to −3.5° during the beginning of the upstroke and rising back again (Fig. 8g).

Discussion

Thrust and weight support of the bat is generated by the aerodynamic lift (L) of the wing, which is determined by the density of the medium (ρ), the speed of the wing relative to the air (U_{eff}), the wing area (S) and the lift coefficient (C_l) according to the following equation (Anderson, 1991):

$$L = \frac{1}{2}\rho S U_{eff}^2 C_l$$

Each of these factors, except density, is controlled by different parameters of the wing morphology and kinematics. The speed of the wing is determined by the combination of flight speed and flapping speed, with the latter determined by the amplitude and frequency of the wing beat. Wing area can be controlled by retracting or extending the wing. Finally, the lift coefficient depends on the shape of the wing profile (e.g. camber) and the angle of attack, the angle between the chord line and the direction of the airflow that meets the wing. Bats are unique among flying animals in their wing morphology, having highly flexible wings with flexible wing bones and a compliant wing membrane

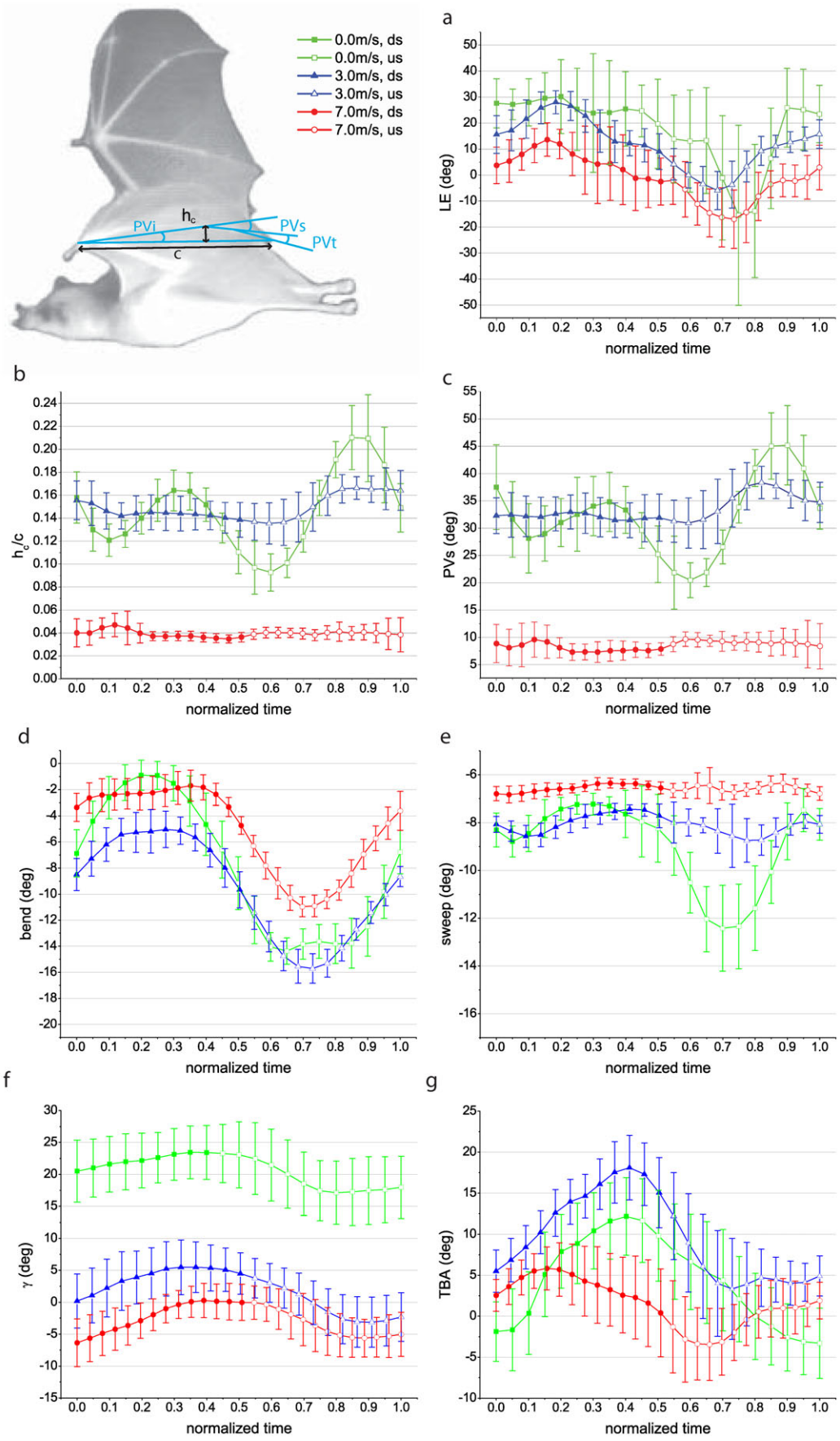

Fig. 8. See next page for legend.

(Swartz et al., 1996; Swartz, 1997). These features enable them to carefully control their wing shape and motion. However, the high degree of control of the wing surfaces may come at a cost of lower aerodynamic flight efficiency in cruising flight since recent studies have shown lower efficiency in bats compared to birds (Muijres et al., 2012b). Our studied bats appeared to actively control multiple parameters, including the wing area, the angle of attack and the camber throughout the wing beat and across flight speeds. At low flight speeds there is a higher variation during the wingbeat in a majority of the measured parameters, generally suggesting a greater level of adjustment at lower compared to higher flight speeds (Figs 7, 8). With decreasing flight speed maintaining lift becomes aerodynamically more demanding and consequently, for example, the wing area, the angle of attack and the camber, which increases lift, increases (Figs 5, 8). In addition, the downstroke Strouhal number (St_d) varies relatively little in the range between 0.2 and 0.4, throughout the studied flight speed range (Fig. 5i). *St* is a dimensionless parameter used as an indicator of the unsteadiness of the airflow (Wang, 2000; Taylor et al., 2003), where values above 0.4 suggest unfavourable vortex shedding (Anderson et al., 1998). The St_d is kept low through changes in the stroke plane angle and the angular velocity of the wing. Below we will discuss in greater detail how the different parameters controlling the lift production are adjusted and compare our results with data from other species.

Controlling speed of the wing relative to the air

The speed of the wing is determined by the combination of flight speed and flapping speed, with the latter being controlled by the amplitude of the wing beat and the wing beat frequency. Wing beat frequency, f, is controlled by muscle contraction frequency and is expected to decrease with increasing body size (Pennycuick, 2008; Bullen and McKenzie, 2002). As expected, the wing beat frequency we found for *L. yerbabuenae* is generally lower than that found for the smaller species *G. soricina* (Lindhe Norberg and Winter, 2006; Wolf et al., 2010). We also found that f decreases with increasing flight speed within the species (Fig. 5f), which agrees with previous studies (Schnitzler, 1971; Norberg, 1976; Aldridge, 1986; Lindhe Norberg and Winter, 2006; Riskin et al., 2010; Wolf et al., 2010; Hubel et al., 2012). The angular amplitude in the stroke plane, θ, varied according to a quadratic relationship with the flight speed, with highest values at low flight speed, decreasing values at medium speed and increasing values at high flight speed (Fig. 5a). As a result, the mean angular velocity ($\bar{\omega} = \theta f$) of the wing in the stroke plane follows a U-shaped pattern (Fig. 5j) with flight speed. A similar pattern was found using data from *G. soricina* (Wolf et al., 2010) (Fig. 5j). This illustrates the need for kinematic changes to maintain weight support when forward flight speed decreases and to generate more thrust to counter the drag increase when flight speed increases. Although other mechanisms, such as modulating wing area and angle of attack, can be used to alter the force generated, lift is proportional to the square of the wing speed but only directly proportional to area and angle of attack. Hence, changing wing speed will have a larger impact on the resulting forces than area and angle of attack. At low flight speed, the relative wing speed during the downstroke is increased relative to the speed during the upstroke reflected in a reduction of the downstroke ratio, further facilitating the generation of higher lift on the downstroke. The minimum $\bar{\omega}$ of *L. yerbabuenae* occurs at ~5.3 m/s (Fig. 5j), which coincides with the speed of maximum lift to drag ratio (*L/D*) estimated from circulation measurements of the vortex wake (5.05 m/s (Muijres et al., 2011)). Interestingly, the minimum $\bar{\omega}$ for *G. soricina* occurs at a lower flight speed (3.4 m/s, Fig. 5j), which also coincides with the maximum *L/D* speed of this species (3.45 m/s (Muijres et al., 2011)). The minimum $\bar{\omega}$ in the stroke plane could therefore be used as an indicator of the optimal flight speed in bats. The $\bar{\omega}$ of the wing should be directly related to the contraction speed of the flight muscles, which in turn determines the efficiency of the muscle (Pennycuick, 2008). Thus, determining if the minimum contraction velocity of the muscles coincides with the maximum efficiency of the flight muscles should be of interest.

Increasing the angular velocity of the wing while keeping the stroke plane constant will result in an increase of the downstroke Strouhal number, St_d (see above). Wolf et al. suggested that the bats may alter the stroke plane to maintain St_d within a favourable region across flight speeds when the demands of increased angular velocity changes (Wolf et al., 2010). We found that the stroke plane angle increased (Fig. 5c) and body angle decreased with increasing flight speed (Fig. 8f) in agreement with previous studies (Wolf et al., 2010; Lindhe Norberg and Winter, 2006; Hubel et al., 2010; Aldridge, 1986; Riskin et al., 2010), but see Hubel et al. for contrasting results (Hubel et al., 2012). This resulted in our bats operating at St_d between 0.2 and 0.3 during the downstroke at all speeds (Fig. 5i), which agrees with the data from *G. soricina* (0.2–0.4 (Wolf et al., 2010)). The maximum St_d occurs between 2 and 3.5 m/s, which is close to the transition flight speed when the backward-flick of the wingtip during the upstroke disappears. At this flight speed the upstroke is expected to be more or less inactive since the wing motion is almost vertical and therefore add little to the weight support (Johansson et al., 2008) and the relatively high St_d could reflect an increased use of unsteady mechanisms during the downstroke to sustain weight support.

Controlling wing area

The area of the wing is largely controlled by the angle between the hand wing and arm bones. Both handwing angles, *PV/IV* and *PIV/III*, stay relatively constant during the downstroke and show only a slight decrease during the upstroke, except at low flight speeds when the handwing flips upside down during supination and there is a decrease of the handwing angle *PIV/III* (Fig. 6e). This appears to be a way to allow for a slack of the membrane, resulting in a more favourable camber of the outer wing during the supinated upstroke. The armwing angles (*H/R* and *R/PV*) show a higher variation than the handwing angles during the wing beat suggesting that wing area is mainly controlled by the changes in the inner wing area (Fig. 6). This is in agreement with the result of Wolf and colleagues, who showed that the span ratio was mainly controlled by changes in the span of the inner wing (*SR* inner wing ~0.4, *SR* hand wing ~0.93) in *G. soricina* (Wolf et al., 2010). During the downstroke the armwing angles decrease with increasing flight speed; the wing area, and hence the effect of wing area on the lift production, decreases as well (Fig. 6). By

Fig. 8. The leading edge angle, camber, *PVs*, bend and sweep, body tilt angle and *TBA* are presented at three different speeds over a normalized wing beat. The bat schemes illustrate the definition of the parameters h_c, *PVs* and *PVt*. The leading edge angle *LE* [°] (**a**), the camber h_c/c (**b**), the angle at the second joint of the 5th finger *PVs* [°] (**c**), the bend [°] (**d**) and the sweep [°] (**e**), body tilt angle γ [°] (**f**) and tail tilt angle relative to the body *TBA* [°] (**g**). The curves are species means ± S.E.M. Filled symbols represent the downstroke, open symbols the upstroke.

mainly adjusting the inner wing area and keeping the outer wing area constant, the outer wing membrane is kept taut during the upstroke. A taut handwing membrane may be a mechanism to avoid an increased drag due to oscillations of a slack membrane (flag effect (Alben and Shelley, 2008)), and may facilitate generation of thrust by the hand wing at the end of the upstroke (Muijres et al., 2011). Thrust generation at the end of the upstroke is demonstrated by the formation of reversed vortex loop in the wake of each wing (Johansson et al., 2008; Muijres et al., 2011), and are associated with the optimal wake topology (minimizing the induced drag) at the *L/D* of these bats (Hall and Hall, 2002), but come at a cost of negative lift (Johansson et al., 2008; Muijres et al., 2011). The inner wing (*plagiopatagium*) contains intrinsic muscles within the membrane and muscles along the leading and trailing edge that may reduce the slack of the membrane (e.g. Norberg, 1972) and thereby mitigate adverse drag effects of a slack membrane when the inner wing span is reduced (Alben and Shelley, 2008).

As mentioned, the span ratio is an indirect measure of how the wing area is controlled during the wing beat. We find that *SR* is lower at flight speeds below the transition speed with the backward flip of the wing i.e. when the wing is flipped upside down and increases to a rather constant plateau at higher flight speeds (Fig. 5d). The almost constant *SR*, with a potential weak negative trend, at higher flight speed is consistent with previous studies of bat flight (Lindhe Norberg and Winter, 2006; Wolf et al., 2010; Hubel et al., 2010; Hubel et al., 2012). In birds *SR* tends to decrease with increasing flight speed and, in comparison with birds, bats tend to have a relatively high *SR* at cruising speed (Tobalske et al., 2007). In birds the *SR* has been seen as a way to control the relative contribution of the downstroke and upstroke to the lift and thrust generated, based on a constant circulation model (e.g. Pennycuick, 1989b). However, in bats the circulation is not constant throughout the wing beat (Hedenström et al., 2007; Johansson et al., 2008; Muijres et al., 2011; Hubel et al., 2010; Hubel et al., 2012) and the upstroke function is different in bats compared to birds; bats generate thrust and negative lift at the end of the upstroke as manifested in the reversed vortex loops (see above) (Hedenström et al., 2007; Johansson et al., 2008; Muijres et al., 2011; Hubel et al., 2010; Hubel et al., 2012), which have not been found in bird wakes (Johansson and Hedenström, 2009; Muijres et al., 2012a). Consequently, generalization of how the *SR* should vary across flight speed in both birds and bats is not recommended.

Controlling the lift coefficient

When it comes to controlling the lift coefficient of the wing we consider angle of attack and camber to be among the most important factors (Anderson, 1991). Both factors have been shown to be related to the circulation (Γ) found in the wake, and hence the lift coefficient of the wing ($C_l = 2\Gamma/Uc$), of *G. soricina* also at very high values of camber and angle of attack (Wolf et al., 2010). Although steady aircraft airfoils show stall and loss of lift already above an angle of attack of about 15° at these Reynolds numbers (Laitone, 1997), the bats operate at mean downstroke angles of attack up to 50° (Aldridge, 1986; Norberg, 1976; Riskin et al., 2010; Wolf et al., 2010) without apparent lift loss (Wolf et al., 2010). This suggests that bats must have some mechanisms to maintain lift throughout the downstroke at these high angles of attack. Flow visualizations have shown that *G. soricina* uses leading edge vortices (Muijres et al., 2008) that stay attached to the wing during the downstroke, which may contribute up to 40% of the total lift at mid-downstroke at low flight speeds (~1 m/s).

A higher angle of attack produces higher lift, but also higher drag, and therefore the bats are expected to reduce the angle of attack with increasing flight speed when the demand of a high lift coefficient is reduced. As expected, both the maximum and average angles of attack during the downstroke decreased with increasing flight speed in our study (Fig. 5g,h), which corresponds to the pattern of how the force coefficient varies with speed in this species (Muijres et al., 2011). The same pattern of decreasing angle of attack with increasing flight speed is found in *G. soricina* (Wolf et al., 2010), and is also implicated by other studies (Aldridge, 1986; Hubel et al., 2010; Riskin et al., 2010; Hubel et al., 2012). However, both maximum and mean angles of attack at intermediate and high flight speeds are lower for *L. yerbabuenae* than for *G. soricina*. A lower angle of attack in *L. yerbabuenae* than in *G. soricina* may reflect that the wings operate more efficiently (higher *L/D*) at higher flight speeds, generating sufficient lift with a lower angle of attack and thus at a lower drag (Muijres et al., 2011).

A compliant wing membrane controlled by multiple jointed fingers allow for both passive and detailed active control of the camber of the wing. Passive mechanisms would include aeroelastic bulging of the wing membrane, while active mechanisms would include bending of the fingers and contraction of intramembraneous muscles. As with the angle of attack, a high camber results in a high lift coefficient, but also in an increased drag of the wing (Anderson, 1991). With increasing flight speed the requirements for a high lift coefficient is reduced and a decrease of the camber reduces the increasing profile drag (Laitone, 1997).

The tail-to-body angle, *TBA*, is a potential mechanism for active control of the camber of the innermost part of the wing, although *TBA* has been proposed to follow the wing motion passively (Eisentraut, 1936). The *TBA* shows the highest angles (resulting in the highest camber) during the downstroke and with low or negative values during the upstroke (Fig. 8g). The relationship with flight speed is more complicated than the other measures of wing camber, with the highest values at intermediate flight speeds. The reason for this is not clear at this point, but could relate to the fact that the innermost part of the wing is aerodynamically relatively inactive at the lowest flight speed range due to the low speed of the flow across the wing, but potentially more important at intermediate flight speeds when in addition the upstroke is more or less inactive (Johansson et al., 2008).

Bending of the 5th digit would correspond to the most direct way of controlling the camber of a wing. The angle at the inner joint (*metacarpal–phalangeal*) of the 5th digit (*PVs*) is highly correlated with the camber and can thus be used as an indirect measurement (Fig. 8b,c). The angle at the outer joint (between the two phalanges) of the 5th finger (*PVt*), on the other hand, seems to show no clear pattern. It is possible that this latter result is a consequence of the animal actively controlling the wing to adjust the vortex shedding at the trailing edge or that variation in angle is a passive aeroelastic response without an active control mechanism. As expected, we found decreasing camber and *PVs* angle with increasing flight speed consistent with previous results (Riskin et al., 2010; Wolf et al., 2010), and the variation throughout the wing stroke was also greatest at low flight speeds.

A peculiar result is that at low flight speeds the maximum camber is reached during the upstroke (Fig. 8b). It is not clear if the high camber during the upstroke has any aerodynamic function for the inner wing, since the speed of the air relative to the wing is relatively low during the upstroke, or if it is instead only a consequence of the twist of the trailing edge during the supination of the handwing to generate more favourable conditions at the outer wing. Further studies of the detailed aerodynamics of the upstroke are needed to determine the consequences of the high camber observed.

The *dactylopatagium brevis* and the *dactylopatagium minus* have been suggested to act as control devices for the flow over the wing by functioning as leading edge flaps (Norberg, 1990). The deflection of a leading edge flap increases the effective camber of the wing. We found an increasing deflection of the leading edge with decreasing speed hence suggesting a higher lift coefficient at lower flight speeds (Fig. 8a). The deflection of the leading edge flap also increases the curvature of the front part of the wing, which would promote the separation of the flow, similar to what has been suggested as the function of the alula in landing steppe eagles (Carruthers et al., 2007), and facilitates the generation of the leading edge vortex used at low speeds (see above). At mid-upstroke there is a more pronounced decrease in the leading edge angle at low flight speeds than at higher flight speeds. Lower, or even negative, deflection of the leading edge flap occurs during the supination of the handwing, where an upward flexion of the leading edge would generate a more suitable wing profile i.e. reversed camber and hence higher force production since the handwing is operating upside down. The angle of the leading edge flap showed high variation. It is possible that this variation results from the small distance between the tip of the 2nd digit and the inner segment of the 3rd digit or difficulty in locating the points during the digitization, but it could also be a highly controllable mechanism to adjust the flow over the wing during flight.

At the outermost part of the wing the fingers run more closely in the spanwise direction than in the chordwise direction, making camber control by the fingers, similar to the 5th digit, less likely. A passive mechanism for camber control at the outermost part of the wing may be the bending and sweeping of the wing tip. Due to the flexibility of the finger bones (Swartz, 1997; Swartz et al., 2006) both the bend and sweep of the wingtip are affected by the aerodynamic forces on the wing and could passively affect the camber of the wing (Neuweiler, 2000). An upward bend of the wing tip, which is swept rearwards relative to the rotational axis of the third digit, indicates a positive camber of the outer wing. Since the bend at zero loading was not measured in this study, the values we present here are relative. During the downstroke the wing tip is bent upwards relative to the mean position during the wing beat (Fig. 8d) (corresponding to the pattern of the force generated during the wingbeat (Muijres et al., 2011)), indicating an increased effective camber. The bend during the upstroke is reversed compared to the downstroke, most likely as a result of the inverted pressure at the outer wing during the upstroke.

Conclusion

Maintaining weight support and generating thrust to overcome drag are the main challenges in level flapping flight. The aerodynamic lift generated by a wing is proportional to the square of the local speed of the wing, i.e. the vector sum of the forward flight speed and the flapping speed of the wing. Altering flight speed changes the forward velocity component over the wing, and we expect the bats to alter the kinematics to sustain weight support and to generate sufficient thrust. The unique flexibility and controllability of bat wings suggest a multitude of mechanisms to control the lift generated by the wing. We find that all parameters that adjust lift, namely flapping speed, wing area and the lift coefficient, are adjusted when changing flight speed. The flapping speed of the wing, which has the largest impact on lift production, shows a U-shaped pattern across flight speed. Wing area is highest during the downstroke and also increases with decreasing flight speed. The lift coefficient is determined by the camber and angle of attack of the wing, which both increase with decreasing flight speed. The angle of attack is highest during the downstroke and at low flight speeds and hovering, increasing the probability of unsteady mechanisms being used to further increase the lift (Muijres et al., 2008). Our examination of the camber across the wing span show an increasing camber with decreasing speed for all positions along the span, until the transition speed when the wing is flipped upside down with a more complex change of camber at lower speeds. The results also suggest that the bats adjust kinematics to control the flow over the wings and to reduce the drag generated. The bats alter their stroke plane angle, suggested to maintain favourable flow characteristics across flight speeds (Wolf et al., 2010), as indicated by the low downstroke Strouhal number, when demands on the force production and angular velocity of the wing changes. The hand wing is kept taut during the upstroke, most likely reducing drag, while the changes in inner wing area may be accomplished while keeping the membrane taut by contraction of intrinsic muscles of the wing membrane. Our results thus strongly suggest that bats utilize their unique capabilities by adjusting wing morphology to control the flow over the wings across the range of flight speeds studied here.

The optimal flight speed of a species should be selected for by its life history traits. Here we compared the kinematics of a long distance migrant and commuting bat, *L. yerbabuenae*, with that of a hovering specialist, *G. soricina*, that had previously been shown to differ in aerodynamic performance (Muijres et al., 2011). The optimal flight speed, based on the maximum lift to drag ratio estimated from quantitative wake studies (Muijres et al., 2011), corresponds to the flight speed of minimum angular velocity of the wing in the stroke plane. It would thus be of great interest to test if this relationship holds for more species, since the kinematic parameters used are easier to obtain than the quantitative wake data and therefore could provide a basis for optimal flight speed estimates for comparative studies not concerned with the wake *per se*.

There are still several questions to be examined. For example, our study shows individual variation in some parameters and our low sample size thus caution against over interpretation, but suggests that individual variation require further attention. Interestingly, most of the parameters showing individual differences control the angular flapping velocity of the wing, which does not differ between individuals, and suggest a potentially different way of obtaining the same relevant output. Selecting the variables for comparison between individuals is thus important. In addition, more bat species of different size need to be studied for a better understanding of scaling effects and generality of our findings. Another natural next step is to connect the kinematics directly to the aerodynamics. This should provide a better understanding of the

effects of the individual mechanisms of wing shape control on the resulting force generation.

Acknowledgements

The research was funded by the German Academic Exchange Service (DAAD) to R.v.B., the Swedish Research Council to A.H. and L.C.J., the Royal Physiographic Society in Lund to L.C.J., and received support from the Centre for Animal Movement Research (CAnMove) financed by a Linnaeus grant (349-2007-8690) from the Swedish Research Council and Lund University. The experiments were approved by the Lund University ethical board (M153-05).

Competing Interests

The authors have no competing interests to declare.

References

Alben, S. and Shelley, M. J. (2008). Flapping states of a flag in an inviscid fluid: bistability and the transition to chaos. *Phys. Rev. Lett.* **100**, 074301.

Aldridge, H. D. J. N. (1986). Kinematics and aerodynamics of the greater horseshoe bat, *Rhinolophus ferrumequinum*, in horizontal flight at various flight speeds. *J. Exp. Biol.* **126**, 479-497.

Anderson, J. D. (1991). *Fundamentals Of Aerodynamics*, p.772. New York: McGraw-Hill.

Anderson, J. M., Streitlien, K., Barrett, D. S. and Triantafyllou, M. S. (1998). Oscillating foils of high propulsive efficiency. *J. Fluid Mech.* **360**, 41-72.

Bullen, R. D. and McKenzie, N. L. (2002). Scaling bat wingbeat frequency and amplitude. *J. Exp. Biol.* **205**, 2615-2626.

Carruthers, A. C., Thomas, A. L. R. and Taylor, G. K. (2007). Automatic aeroelastic devices in the wings of a steppe eagle *Aquila nipalensis*. *J. Exp. Biol.* **210**, 4136-4149.

Eisentraut, M. (1936). Beitrag zur Mechanik des Fledermausfluges. *Z. Wiss. Zool.* **148**, 159-188.

Hall, K. C. and Hall, S. R. (2002). A rational engineering analysis of the efficiency of flapping flight. In *Fixed And Flapping Wing Aerodynamics For Micro Air Vehicle Application* (*Progress In Astronautics And Aeronautics*), Vol. 195 (ed. T. J. Mueller), pp. 249-274. Reston, VA: American Institute of Aeronautics and Astronautics.

Hedenström, A., Johansson, L. C., Wolf, M., von Busse, R., Winter, Y. and Spedding, G. R. (2007). Bat flight generates complex aerodynamic tracks. *Science* **316**, 894-897.

Horner, M. A., Fleming, T. H. and Sahey, C. T. (1998). Foraging behaviour and energetics of a nectar-feeding bat, *Leptonycteris curasoae* (Chiroptera: Phyllostomidae). *J. Zool.* **244**, 575-586.

Hubel, T. Y., Riskin, D. K., Swartz, S. M. and Breuer, K. S. (2010). Wake structure and wing kinematics: the flight of the lesser dog-faced fruit bat, *Cynopterus brachyotis*. *J. Exp. Biol.* **213**, 3427-3440.

Hubel, T. Y., Hristov, N. I., Swartz, S. M. and Breuer, K. S. (2012). Changes in kinematics and aerodynamics over a range of speeds in *Tadarida brasiliensis*, the Brazilian free-tailed bat. *J. R. Soc. Interface* **9**, 1120-1130.

Johansson, L. C. and Hedenström, A. (2009). The vortex wake of blackcaps (*Sylvia atricapilla* L.) measured using high-speed digital particle image velocimetry (DPIV). *J. Exp. Biol.* **212**, 3365-3376.

Johansson, L. C., Wolf, M., von Busse, R., Winter, Y., Spedding, G. R. and Hedenström, A. (2008). The near and far wake of Pallas' long tongued bat (*Glossophaga soricina*). *J. Exp. Biol.* **211**, 2909-2918.

Kenward, M. G. and Roger, J. H. (1997). Small sample inference for fixed effects from restricted maximum likelihood. *Biometrics* **53**, 983-997.

Laitone, E. V. (1997). Wind tunnel tests of wings at Reynolds numbers below 70 000. *Exp. Fluids* **23**, 405-409.

Lindhe Norberg, U. M. and Winter, Y. (2006). Wing beat kinematics of a nectar-feeding bat, *Glossophaga soricina*, flying at different flight speeds and Strouhal numbers. *J. Exp. Biol.* **209**, 3887-3897.

Muijres, F. T., Johansson, L. C., Barfield, R., Wolf, M., Spedding, G. R. and Hedenström, A. (2008). Leading-edge vortex improves lift in slow-flying bats. *Science* **319**, 1250-1253.

Muijres, F. T., Johansson, L. C., Winter, Y. and Hedenström, A. (2011). Comparative aerodynamic performance of flapping flight in two bat species using time-resolved wake visualization. *J. R. Soc. Interface* **8**, 1418-1428.

Muijres, F. T., Bowlin, M. S., Johansson, L. C. and Hedenström, A. (2012a). Vortex wake, downwash distribution, aerodynamic performance and wingbeat kinematics in slow-flying pied flycatchers. *J. R. Soc. Interface* **9**, 292-303.

Muijres, F. T., Johansson, L. C., Bowlin, M. S., Winter, Y. and Hedenström, A. (2012b). Comparing aerodynamic efficiency in birds and bats suggests better flight performance in birds. *PLoS ONE* **7**, e37335.

Neuweiler, G. (2000). *The Biology Of Bats*. New York: Oxford University Press.

Norberg, U. M. (1972). Bat wing structures important for aerodynamics and rigidity (Mammalia, chiroptera). *Zoomorphology* **73**, 45-61.

Norberg, U. M. (1976). Aerodynamics, kinematics, and energetics of horizontal flapping flight in the long-eared bat *Plecotus auritus*. *J. Exp. Biol.* **65**, 179-212.

Norberg, U. M. (1990). *Vertebrate Flight: Mechanics, Physiology, Morphology, Ecology And Evolution* (*Zoophysiology Series*), Vol. 27. Berlin; New York: Springer-Verlag.

Pennycuick, C. J. (1989a). *Bird Flight Performance: A Practical Calculation Manual*. Oxford (UK); New York: Oxford University Press.

Pennycuick, C. J. (1989b). Span-ratio analysis used to estimate effective lift:drag ratio in the double-crested cormorant *Phalacrocorax auritus* from field observations. *J. Exp. Biol.* **142**, 1-15.

Pennycuick, C. J. (2008). *Modelling The Flying Bird*, p. 480. Amsterdam: Academic Press.

Pennycuick, C. J., Alerstam, T. and Hedenström, A. (1997). A new low-turbulence wind tunnel for bird flight experiments at Lund University, Sweden. *J. Exp. Biol.* **200**, 1441-1449.

Riskin, D. K., Iriarte-Díaz, J., Middleton, K. M., Breuer, K. S. and Swartz, S. M. (2010). The effect of body size on the wing movements of pteropodid bats, with insights into thrust and lift production. *J. Exp. Biol.* **213**, 4110-4122.

Schnitzler, H.-U. (1971). Fledermäuse im Windkanal. *Z. Vgl. Physiol.* **73**, 209-221.

Swartz, S. M. (1997). Allometric patterning in the limb skeleton of bats: implications for the mechanics and energetic of powered flight. *J. Morphol.* **234**, 277-294.

Swartz, S. M. and Middleton, K. M. (2008). Biomechanics of the bat limb skeleton: scaling, material properties and mechanics. *Cells Tissues Organs* **187**, 59-84.

Swartz, S. M., Groves, M. S., Kim, H. D. and Walsh, W. R. (1996). Mechanical properties of bat wing membrane skin. *J. Zool.* **239**, 357-378.

Swartz, S. M., Bishop, K. and Ismael-Aguirre, M.-F. (2006). Dynamic complexity of wing form in bats: implications for flight performance. In *Functional And Evolutionary Ecology Of Bats* (ed. Z. Akbar, G. F. McCracken and T. H. Kunz). Oxford (UK); New York: Oxford University Press.

Taylor, G. K., Nudds, R. L. and Thomas, A. L. R. (2003). Flying and swimming animals cruise at a Strouhal number tuned for high power efficiency. *Nature* **425**, 707-711.

Thollesson, M. and Norberg, U. M. (1991). Moments of inertia of bat wings and body. *J. Exp. Biol.* **158**, 19-35.

Tobalske, B. W., Warrick, D. R., Clark, C. J., Powers, D. R., Hedrick, T. L., Hyder, G. A. and Biewener, A. A. (2007). Three-dimensional kinematics of hummingbird flight. *J. Exp. Biol.* **210**, 2368-2382.

Wang, Z. J. (2000). Vortex shedding and frequency selection in flapping flight. *J. Fluid Mech.* **410**, 323-341.

Wilkinson, G. S. and Fleming, T. H. (1996). Migration and evolution of lesser long-nosed bats *Leptonycteris curasoae*, inferred from mitochondrial DNA. *Mol. Ecol.* **5**, 329-339.

Wolf, M., Johansson, L. C., von Busse, R., Winter, Y. and Hedenström, A. (2010). Kinematics of flight and the relationship to the vortex wake of a Pallas' long tongued bat (*Glossophaga soricina*). *J. Exp. Biol.* **213**, 2142-2153.